Luce *et al. Earth, Planets and Space (2018) 70:207*
https://doi.org/10.1186/s40623-018-0979-1

Earth, Planets and Space

FULL PAPER

Open Access

Turbulence kinetic energy dissipation rates estimated from concurrent UAV and MU radar measurements

Hubert Luce[1], Lakshmi Kantha[2], Hiroyuki Hashiguchi[3]*, Dale Lawrence[2] and Abhiram Doddi[2]

Abstract

We tested models commonly used for estimating turbulence kinetic energy dissipation rates ε from very high frequency stratosphere–troposphere radar data. These models relate the root-mean-square value σ of radial velocity fluctuations assessed from radar Doppler spectra to ε. For this purpose, we used data collected from the middle and upper atmosphere (MU) radar during the Shigaraki unmanned aerial vehicle (UAV)—radar experiment campaigns carried out at the Shigaraki MU Observatory, Japan, in June 2016 and 2017. On these occasions, UAVs equipped with fast-response and low-noise Pitot tube sensors for turbulence measurements were operated in the immediate vicinity of the MU radar. Radar-derived dissipation rates ε estimated from the various models at a range resolution of 150 m from the altitude of 1.345 km up to the altitude of ~ 4.0 km, a (half width half power) beam aperture of 1.32° and a time resolution of 24.6 s, were compared to dissipation rates (ε_U) directly obtained from relative wind speed spectra inferred from UAV measurements. Firstly, statistical analysis results revealed a very close relationship between enhancements of σ and ε_U for $\varepsilon_U \gtrsim 10^{-5}$ m^2 s^{-3}, indicating that both instruments detected the same turbulent events with ε_U above this threshold. Secondly, ε_U was found to be statistically proportional to σ^3, whereas a σ^2 dependence is expected when the size of the largest turbulent eddies is smaller than the longitudinal and transverse dimensions of the radar sampling volume. The σ^3 dependence was found even after excluding convectively generated turbulence in the planetary boundary layer and below clouds. The best agreement between ε_U and radar-derived ε was obtained with the simple formulation based on dimensional analysis $\varepsilon = \sigma^3/L_c$ where $L_C \approx$ 50–70 m. This empirical expression constitutes a simple way to estimate dissipation rates in the lower troposphere from MU radar data whatever the sources of turbulence be, in clear air or cloudy conditions, consistent with UAV estimates.

Keywords: VHF radar, Unmanned aerial vehicle, Atmospheric turbulence, Energy dissipation rate, Outer scales of turbulence, Doppler variance

Introduction

Turbulence kinetic energy (TKE) dissipation rate ε is a fundamental parameter indicative of the strength of turbulence. Dissipation rates of atmospheric turbulence can be potentially retrieved from stratosphere–troposphere (ST) radars operating in VHF (e.g., Hocking 1983, 1985, 1986, 1999; Fukao et al. 1994; Hocking and Hamza 1997; Nastrom and Eaton 1997; Li et al. 2016) and UHF bands (e.g., Sato and Woodman 1982; Cohn 1995; Bertin et al. 1997; Wilson et al. 2005 and references therein). Because ST radars can be used for detecting turbulence in the free atmosphere (above the atmospheric boundary layer), standard models are based on the assumption that turbulence results from shear flow instabilities in a stably stratified background (e.g., Fukao et al. 1994; Kurosaki et al. 1996; Nastrom and Eaton 1997). For such turbulence, the stable stratification limits the size of the largest turbulent eddies and damps vertical motions, leading to the definition of various outer scales of stratified turbulence (e.g., Weinstock 1978a, b, 1981). Additional key assumptions used to retrieve turbulence parameters from radar data

---

*Correspondence: hasiguti@rish.kyoto-u.ac.jp
[3] Research Institute for Sustainable Humanosphere, Kyoto University, Kyoto, Japan
Full list of author information is available at the end of the article

are that isotropic turbulence, following the Kolmogorov–Obukhov–Corrsin (KOC) model, exists at smaller scales in the inertial subrange and that the Bragg wavelength of radar backscatter lies within this inertial subrange. Estimation of ε is therefore based on the measurement of radar Doppler spectral width assuming that part of the spectral broadening results from isotropic turbulent motions in the radar measurement volume (the so-called Doppler method). Indirect estimates of ε can also be obtained from the estimates of refractive index structure constant C_n^2 from radar echo power (e.g., Gage and Balsley 1978; Cohn 1995; Hocking and Mu 1997; Hocking 1999) but that is beyond the scope of the present work.

The purpose of the present work is to show the results of comparisons between ε estimates made from middle and upper atmosphere (MU) radar data in the lower troposphere using existing formulations and direct in situ estimates of ε obtained from small unmanned aerial vehicles (UAVs) equipped with high-frequency sampling and fast-response Pitot (airspeed) sensors (Kantha et al. 2017). The potential of UAVs for characterizing turbulence properties was thoroughly described by Lawrence and Balsley (2013). Contrary to the radar technique which samples the atmosphere inside a volume at a fixed location, the UAV has the potential to probe all the space occupied by a turbulent layer/patch and may be a better tool for identifying the dimensions of a turbulent volume and for estimating outer scales.

The datasets were collected during two field campaigns, called the Shigaraki UAV Radar Experiments (ShUREX), in May–June 2016 and June 2017 at the Shigaraki MU observatory in Japan. Kantha et al. (2017) described the instruments and configurations used during a previous ShUREX campaign in June 2015. The instrumental setup did not significantly change in 2016 and 2017, except for the use of higher-frequency sampling and lower-noise turbulence sensors. The CU DataHawk UAVs flew in the immediate vicinity of the radar (within a horizontal distance of ~ 1.0 km) and up to altitudes of ~ 4.0 km above the sea level (ASL). Selected data from 39 science flights (16 in 2016 and 23 in 2017) were used for the present study. "Instruments and data" section describes briefly the MU radar and DataHawk UAV and the observational configurations used during the campaigns. "Theoretical bases and practical methods of ε estimation" section presents the theoretical expressions used for retrieving TKE dissipation rates from radar and UAV data and describes in detail the practical methods. As summarized by Hocking (1999), the Doppler method leads to different analytical expressions according to hypotheses made on the properties of turbulence and according to the radar specifications. In the present work, we will focus on the most commonly used expressions without describing their derivations. The underlying hypotheses will be shortly recalled. More details can be found in Kantha et al. (2018) "Comparisons between ε_U and ε from the radar models" section presents the results of comparisons between the various dissipation rate estimates. These results are discussed in "Discussion" section, and conclusions are presented in "Conclusions" section.

Table 1 MU radar parameters used during ShUREX 2016 and 2017 campaigns

Parameter	
Beam directions	(0°, 0°),(0°, 10°), (90°, 10°)
Radar frequencies (MHz)	46.00, 46.25, 46.50, 46.75, 47.00
Interpulse period (μs)	400
Subpulse duration (μs)	1
Pulse coding	16-bit optimal complementary code
Range resolution (m)	150
Height sampling (FII) (m)	5
Number of gates	128
Coherent integration number	32
Incoherent integration number	– (time series)
Number of FFT points	128
Acquisition time for one profile (s)	24.57
Profile acquired every: (s)	6.144
Nyquist frequency (Hz)	2.60
Velocity aliasing (m s^{-1})	8.4

Instruments and data

MU radar

The MU radar is a 46.5 MHz beam-steering Doppler pulsed radar located at the Shigaraki MU Observatory (34.85°N, 136.10°E) in Japan (Fukao et al. 1990). The radar parameters used during the ShUREX 2016 and 2017 campaigns are listed in Table 1. The radar was operated in range-imaging mode using frequency diversity (see Luce et al. 2006) at vertical and two oblique incidences (10° off zenith toward North and East) for high-resolution echo power observations. The radar parameters were set up so that one high-resolution profile of echo power at vertical incidence was acquired from the altitude of 1.270 km up to 20.465 km (ASL) at a dwell time of 24.57 s, every 6.144 s (see Table 1). The radar data were also processed at a standard range resolution of 150 m for retrieving signal-to-noise ratios (SNR), radial winds and spectral widths using the moment method (e.g., Yamamoto et al. 1988).

CU DataHawk UAV

The ShUREX campaign and the characteristics of the CU DataHawk UAVs and onboard sensors are described by Kantha et al. (2017). The UAVs were equipped with a custom autopilot programmed to execute a preplanned trajectory near the MU radar. The UAVs could also be commanded to sample interesting atmospheric features revealed by the MU radar in near real time. For the present purpose, we only consider measurements performed during "vertical" ascents and descents. When moving up or down, the UAVs were flying along helical trajectories ~ 100–150 m in diameter at a typical vertical velocity rate of ~ 2 m s^{-1}. The maximum flight altitude was limited to ~ 4.0 km ASL by both battery capabilities and air traffic regulations. Among 41 flights performed during the 2016 campaign, 16 science flights provided (totally or partially) valuable data for comparisons with MU radar data. Hereafter, they will be denoted 'FLT16-xx', where '16' refers to the year and 'xx' is the flight number. In 2017, 23 science flights were available for analysis.

The UAVs were equipped with a variety of sensors for atmospheric measurements (Kantha et al. 2017). Among these sensors, a commercial IMET sonde provided measurements of pressure, temperature and relative humidity (PTU) at 1 Hz. Velocity of the air flow relative to the UAV was measured by a fast-response Pitot-static tube and a differential pressure sensor, with the Pitot tube mounted at a height of 3 cm above the vehicle so as to project into the free stream above the aerodynamic boundary layer. This sensor was sampled at an effective rate of 400 Hz. At the nominal airspeed of 14 m s^{-1}, the digital resolution was 0.042 m s^{-1} (see Kantha et al. 2017). In addition, a fast-response (< 1 ms) cold wire sensor was also available for temperature measurements sampled at 800 Hz.

There were too many flights to describe their characteristics in detail. Most of the flights had ascents and descents (denoted by 'A' and 'D' when necessary) sometimes separated by horizontal legs of various durations (e.g., FLT16-22 and FLT16-38). Unanticipated blocking of the Pitot tube (used also by the autopilot for flight control) by precipitation sometimes produced short time span (~ a few tens of seconds) downward motions during ascents (e.g., FLT16-05, FLT16-15). These sources of aberrant data points were manually removed.

The meteorological conditions were checked every day before deciding to launch UAVs or not since they cannot fly during rainy conditions and strong winds (> 10–15 m s^{-1}). The state of the lower atmosphere during the flights could be known from the available data without additional meteorological information. Indeed, among other things, the relative humidity measurements made by humidity sensors onboard UAV indicated flight in clouds and the radar images provided precise information on the vertical extent and evolution of the convective boundary layer when it exceeded the altitude of the first radar sampling gate. Therefore, turbulence associated with dry or saturated convections could be easily identified from the datasets and could be removed from statistics when focusing on stratified and clear air turbulence only. Actually, the weather was almost clear through the observations above the convective boundary layer.

Theoretical bases and practical methods of ε estimation

Theoretical expressions of ε from radar data

From a dimensional analysis, the dissipation rate (assuming isotropy) can be inferred from:

$$\varepsilon \sim \left\langle w'^2 \right\rangle^{3/2} / L$$

where $\left\langle w'^2 \right\rangle$ is the variance of vertical wind fluctuations and L is a typical scale of the turbulent eddies. A rms value σ of radial turbulent velocity fluctuations can be obtained from the measured Doppler spectral width after removing non-turbulent contributions to the spectral broadening (see "Appendix") (e.g., Hocking 1986; Fukao et al. 1994; Naström 1997; Dehghan and Hocking 2011). Similarly to the above expression, we can write:

$$\varepsilon_R = \sigma^3 / L_c \tag{1}$$

where L_c has the dimension of a turbulence scale. Expression (1) is only indicative, but it will be first used in order to see if a particular value of L_c emerges from our dataset.

In practice, two main expressions are used for estimating ε from the Doppler spectral width, based on more elaborated models. When the outer scale L_{out} of turbulence is small compared to the horizontal and transverse dimensions of the radar sampling volume, $2a$, $2b$[1] we have (e.g., Hocking 1983, 1999, 2016):

$$\varepsilon_N = C\sigma^2 N \tag{2}$$

where C is a constant ($= 0.5 \pm 0.25$) according to Hocking (2016). $C = 0.47$, sometimes used in the literature, was applied for producing the figures. The parameter N is the Brunt–Väisälä frequency. Expression (2) has been established for characterizing turbulence in stratified conditions only [whereas expression (1) is always valid]. Various definitions of outer scales of stably stratified turbulence have been proposed in order to obtain dissipation rate expressions in the form of (2) (e.g., Weinstock 1978a, b, 1981). Expression (2) is virtually identical to the theoretical expression given by Weinstock (1981) obtained by integrating the spectrum of inertial turbulence down to the buoyancy wavenumber $k_{\text{B}} = N / \sqrt{\left\langle w'^2 \right\rangle}$ so that $\varepsilon \approx 0.5 \left\langle w'^2 \right\rangle N$. Hocking (2016) makes use of the one-dimensional transverse spectrum [expression (7.42)] whose integration, by including additional contribution from the buoyancy subrange, leads to

---

[1] $b = \Delta r/2$ ($\Delta r = 150$ m) and $a = \theta_0 z$ where z is altitude (m) and $\theta_0 = 1.32°$ for the MU radar (e.g. Fukao et al. 1994).

an estimate of vertical wind fluctuation variance σ^2 supposed to be measured by the radar. By doing so, Expression (2) is obtained with various values of *C*, coincidently close to the coefficient 0.5 of the Weinstock model. Kantha et al. (2018, this issue) used this approach with different conceptual models of turbulence and different definitions of turbulence scales and even generalized it to expressions including the radar volume effects. However, it seems that a definitive modeling is still an open issue.

The alternative approach proposed by, e.g., Frisch and Clifford (1974) and Labitt (1979) considers the role of spatial low-pass band filter played by the radar volume, valid if $L_{\text{out}} \gg 2a, 2b$. The White et al. (1999) formulation also considered the effects of the wind advection:

$$\varepsilon_W = \left(\frac{4\pi}{1.6}\right)^{3/2} \frac{\sigma^3}{I^{3/2}} \tag{3}$$

where

$$I \propto \int_0^{\pi/2} \mathrm{d}\phi \int_0^{\pi/2} \sin^3\theta \times \left(b^2\cos^2\theta + a^2\sin^2\theta + \frac{L_H}{12}\sin^2\theta\cos^2\phi\right)^{1/3} \mathrm{d}\theta$$

and $L_H = VT$, where *V* is the mean horizontal wind speed during the dwell time *T*. It is important to note that expression (3) is based on the hypothesis that the radar is sensitive to the three-dimensional longitudinal spectrum of turbulence (see Doviak and Zrnic' 1993, p. 398). Therefore, Eqs. (2) and (3) are not the asymptotic forms (for $L_{\text{out}} \ll 2a, 2b$ and $L_{\text{out}} \gg 2a, 2b$, respectively) of a more general expression. The ε estimates from Eqs. (2) and (3) (i.e., ε_N and ε_W, respectively) will be compared with those derived from UAV data, hereafter noted ε_U in "Comparisons between ε_U and ε from the radar models" section.

Despite its apparent complexity, Eq. (3) has advantages with respect to Eq. (2). ε_W can be estimated solely from the radar data, while ε_N requires estimates of *N* (usually from balloon measurements) or standard climatological values as default values (e.g., Weinstock 1981; Deghan et al. 2014). In addition, ε_W can be used whatever the turbulence source may be (convective or shear flow instabilities), assuming that inertial turbulence is observed and $L_{\text{out}} \gg 2a, 2b$. Finally, ε_N requires, in principle, the estimation of moist N^2 when air is saturated, because saturation modifies the background stability due to latent heat release. This additional difficulty does not seem to have been considered in the studies related to TKE dissipation rate estimates from ST radar data. However, we shall see that the accuracy of N^2 is not an important issue because our analyses reveal a fundamental inadequacy of ε_N. This conclusion goes beyond the problem of estimating N^2 properly.

Equation (3) or similar expressions were used by Gossard et al. (1982) and Chapman and Browning (2001), for example, using UHF radars at similar spatial resolutions as the MU radar and by McCaffrey et al. (2017) at vertical resolution of ~ 25 m.

Practical methods from radar data

The Doppler variance due to turbulent motions was estimated from the Doppler spectra by applying:

$$\sigma^2 \approx \sigma_m^2 - \sigma_b^2 \tag{4}$$

where σ_m^2 is the Doppler variance measured *at vertical incidence*, and σ_b^2 is the variance due to beam-broadening effects.σ^2 was used in order to obtain ε_R, ε_N and ε_W. Equation (4) is very simple compared to the expressions provided by Naström (1997) and Dehghan and Hocking (2011), because only data from the vertical beam are used. At VHF, data collected at vertical incidence are usually avoided because the radar echoes can be strongly affected by (non-turbulent) specular reflectors so that the spectral width is reduced and σ^2 is biased (e.g., Tsuda et al. 1988). However, Eq. (4) has a great advantage, since shear-broadening effects are null or negligible when using a vertical beam. Even though the theoretical effects due to shear-broadening when using data collected at oblique incidences are well-established, the corrections remain challenging in practice, because they require accurate estimates of wind shears, and the wind shear profiles estimated at the radar range resolution may not be representative of shear profiles at higher resolutions (e.g., Figure 5 of Luce et al. 2018). The use of data at vertical incidence will be justified a posteriori in "Comparisons between ε_U and ε from the radar models" section.

The beam-broadening correction σ_b^2 requires the knowledge of horizontal winds estimated from off-vertical beam data, and these winds may not be exactly those at the altitudes sampled by the vertical beam. It is another source of bias (Deghan and Hocking 2011), but difficult to correct in general. However, since the measurements were taken for low altitudes (< 4.5 km), this problem should be minimized here because the sampled altitude differences between the vertical and oblique directions do not exceed a few tens of meters.

Finally, Eq. (4) does not include correction due to gravity wave contributions (e.g., Naström 1997). Here, it is expected to be negligible: the dwell time (~ 25 s) should be sufficient for minimizing their contribution because it is a small fraction of internal gravity wave periods. The details of the practical procedure for estimating σ^2 from Eq. (4) are given in "Appendix".

A complete vertical profile of σ^2 is calculated from time series of ~ 25 s in length every 6.144 s (overlapping

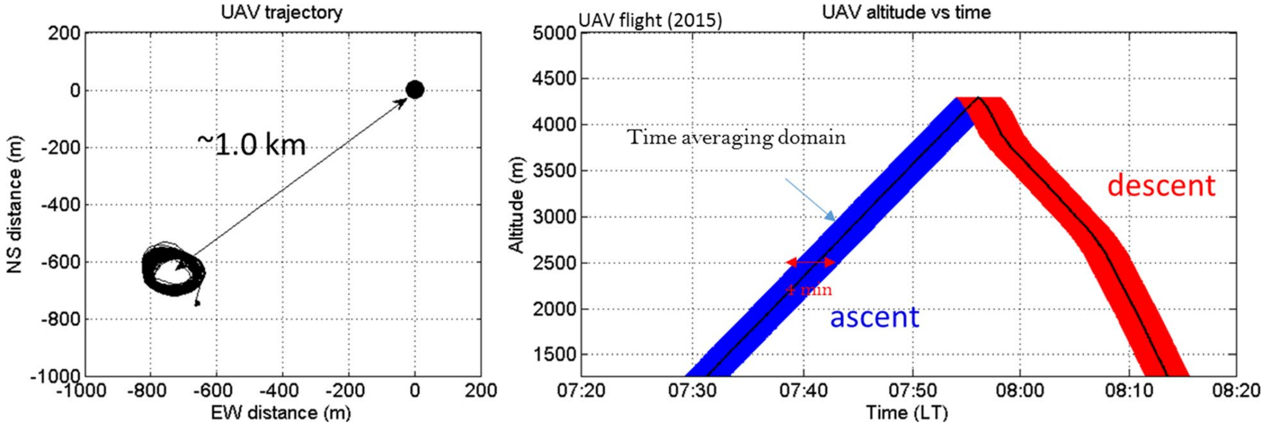

Fig. 1 Schematic representation of the method used for estimating pseudo-vertical profiles of Doppler variances σ^2 from radar data. (Left) Example of horizontal excursion of a UAV with respect to MU radar antenna array location (black dot). (Right) The corresponding UAV altitude versus time (black line). The blue and red areas indicate the time-height domain used for calculating the average of Doppler variances σ^2 during the ascent and descent of the UAV, respectively. Time averaging for a given altitude was arbitrarily performed over 4 min centered at the time when the UAV reached this altitude

of a factor 4) at a vertical resolution of 150 m (see Table 1). For comparison with UAV measurements, it must be realized that the UAV provides data only along a specific altitude versus time trajectory. Figure 1 shows the strategy used for reconstructing pseudo-profiles of σ^2 along the UAV paths. Since the UAVs were flying in the vicinity of the MU radar, we calculated temporal averages of σ^2 ($\langle\sigma^2\rangle$) over a few minutes only (4 min was arbitrarily selected) about the time-height location of the UAV (see Fig. 1), initially assuming that the UAV was flying directly over the radar, so it detected the same atmospheric structures at the same time as the radar. $\langle\sigma^2\rangle$ was estimated for all altitudes sampled by the UAV, using a linear interpolation of the σ^2 profiles (at 150-m resolution) at these altitudes. The same procedure was used for all other radar parameters (e.g., echo power, Luce et al. 2017). The height variations of the pseudo-profiles of $\langle\sigma^2\rangle$ are thus due to a combination of the height and time variations of σ^2. Figure 2 shows an example of pseudo-profiles of $\langle\sigma^2\rangle$ during the ascent A1 and descent D1 of FLT16-15. The gray areas show the rms value of σ^2 during the time averaging for A1 and D1, respectively.

The processing was then refined to account for the actual horizontal offset between UAV and radar by taking time lags due to wind advection into account, assuming frozen advection of the turbulent irregularities by the wind along the wind direction. This often provided higher correlation coefficients between ε_U and the radar-derived ε profiles, especially when the UAV was flying directly upstream of the radar. Yet, because the improvements were quite marginal, the procedure is not described in detail here. Note that time offsets could be avoided by flying in the beam of the radar, but the vehicle produces strong echoes that obliterate the turbulence measurements in the volume of interest, requiring a more complex analysis that considers neighboring times or altitudes (e.g., Scipión et al. 2016).

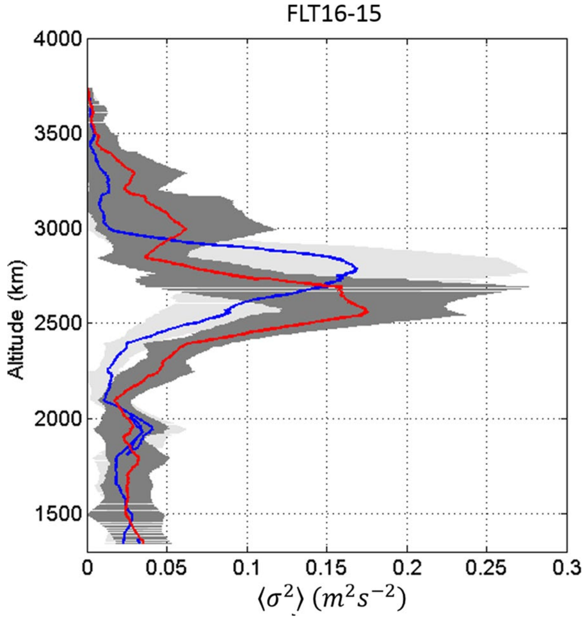

Fig. 2 Example of pseudo-profile of σ^2 calculated according to the procedure shown in Fig. 1 for FLT16-15 A1 (blue) and D1 (red). Light and heavy gray areas show the rms value of σ^2 during the time averaging for A1 and D1, respectively. The zigzag pattern around 2000 m during A1 is due a brief unintended descent of FLT16-15

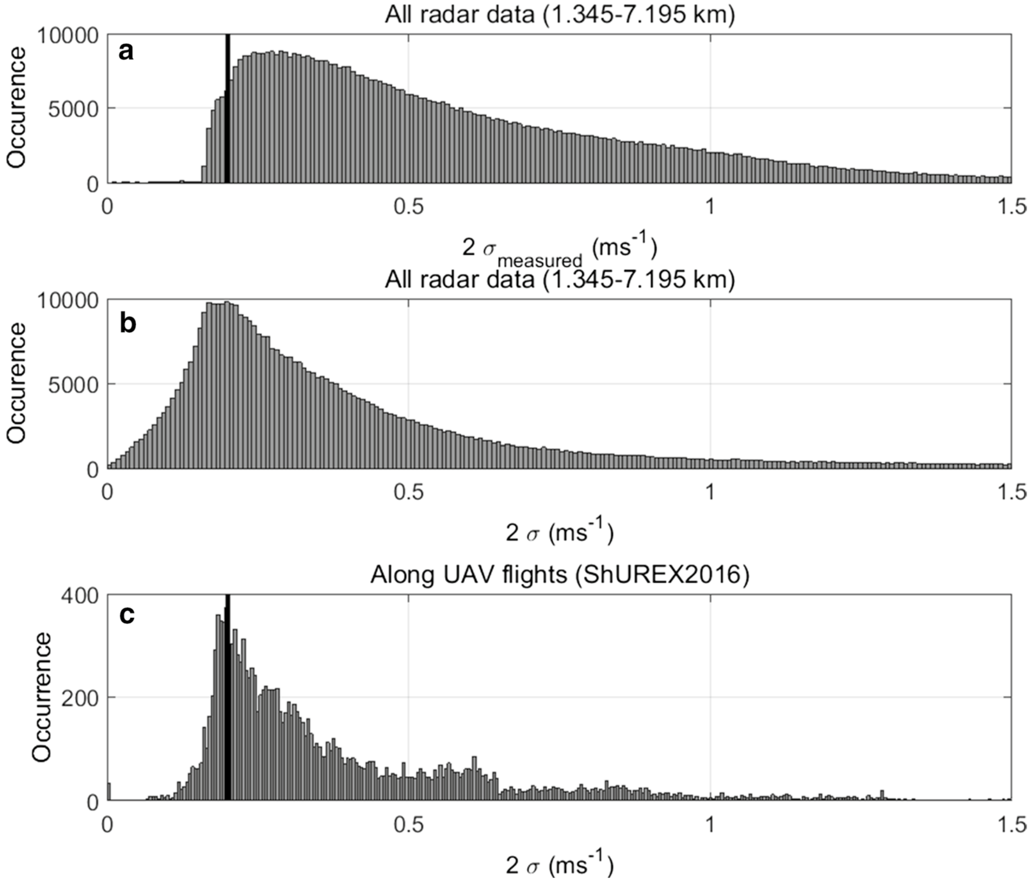

Fig. 3 **a** Histogram of the measured spectral width (m s^{-1}) for all the available radar data surrounding the 2016 UAV flights between 1.345 and 7.195 km (corresponding to the first 40 gates). **b** The corresponding histogram of 2σ (after beam-broadening correction). **c** The histogram of 2σ calculated along the 2016 UAV flight tracks

Figure 3a shows the histogram of the Doppler width $2\sigma_m$ for all the available radar data surrounding the 16 UAV flights of ShUREX2016 in the height range 1.345–7.195 km ASL (corresponding to the first 40 radar gates). Similar statistics were obtained for 2017 data (not shown). It also shows the detection threshold (approximately ~ 0.2 m s^{-1}) for the radar configuration and processing method used. Figure 3b shows the corresponding histogram of 2σ (i.e., the Doppler width after beam-broadening corrections). Due to estimation errors (especially when SNR is low), some σ values can be negative. They are not shown in Fig. 3b. Figure 3c shows the histogram corresponding to the values of 2σ estimated along the UAV flight track (as shown in Fig. 2). The peaks around 0.2 m s^{-1} are of course artificial and result from the minimum detection threshold of the radar. A bias is thus expected when comparing the lowest levels of radar-derived ε with ε_U. In addition, remaining small contaminations by various artifacts may still be present despite careful examination of the spectra (see "Appendix"). They can be a source of important biases for the lowest levels.

It has to be noted that the 2σ values calculated along UAV flight tracks are not affected by estimation errors due to low SNR, because the UAVs did not exceed the altitude of 4.05 km ASL and SNR was always larger than 20 dB below this altitude. In addition, because UAVs flew during relatively weak winds (~ < 10–15 m s^{-1}), the beam-broadening effects were relatively weak. Consequently, the conditions were favorable to errors in 2σ estimates being small and, in particular, very few negative values were obtained in the altitude range of the UAV measurements so that they should not affect the statistics.

Estimation of ε_U from Pitot sensor data

The basics for retrieving ε_U were described by Kantha et al. (2017). Frequency spectra (Eq. 5 of Kantha et al. 2017) were estimated from variance-conserving, Hanning-weighted time intervals of 5 s duration (corresponding to 2000 points

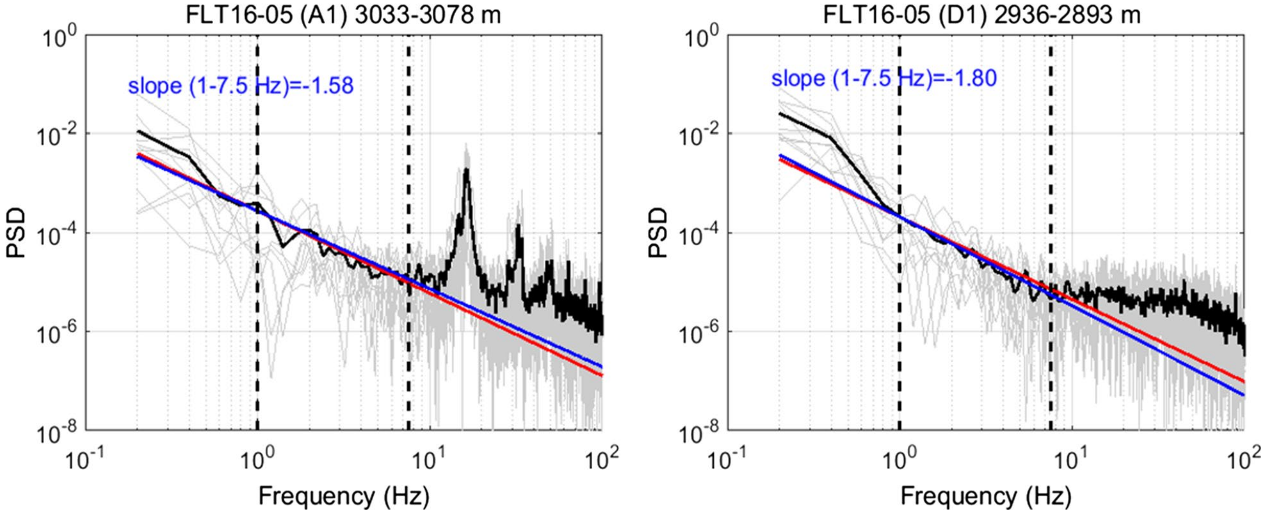

Fig. 4 Example of frequency spectra of *U* up to 100 Hz during the ascent (A1) (left) and descent (D1) (right) of FLT16-05. The black lines show spectra after averaging the 10 spectra in gray lines. The red lines show the — 5/3 inertial subrange slope. The blue lines show the calculated slopes between 1.0 and 7.5 Hz

since the effective sampling rate was 400 Hz) every 2.5 s (corresponding to a successive time interval overlap of 50%). Assuming local isotropy and stationarity of turbulence and using the frozen-advection Taylor hypothesis, the theoretical Kolmogorov 1D power spectral density is of the form (Tatarski 1961; Hocking 1983):

$$S_U(f) = 0.55\varepsilon^{2/3}\left(\frac{\bar{U}}{2\pi}\right)^{2/3} f^{-5/3} \quad (5)$$

[the coefficient 0.55 holds for motions parallel to the mean relative wind]. $\bar{U}$ is the mean relative wind (airspeed). Assuming that the calculated spectrum $\hat{S}_U(f)$ shows an inertial domain (at least in a frequency band), the spectral data will have the frequency dependence:

$$\hat{S}_U(f) = \beta f^{-5/3} \quad (6)$$

An experimental value of ε_U can be obtained by estimating β by fitting spectral data, and equating Eqs. (5) and (6) (e.g., Frehlich et al. 2003; Siebert et al. 2006):

$$\varepsilon_U = \frac{2\pi}{\bar{U}}\left(\frac{\beta}{0.55}\right)^{3/2} \quad (7)$$

Experimental tests in outdoor flight showed that the flow acceleration over the UAV body did not damp the turbulent variations about the mean for the scales of interest, contrary to what it was expected from earlier tests in wind tunnel (which generated much smaller-scale turbulent fluctuations, not shown). Therefore, significant underestimations of energy dissipation rates from these effects are not expected.

Practical methods of estimations from Pitot sensor data

The problem of extracting the dissipation rate from UAV data is now reduced to that of identifying an inertial domain (when it exists) and estimating β. Two different methods were applied with very similar results.

The first method consists in selecting an appropriate frequency band from spectra calculated from 5-s. time series chunks of Pitot data. A careful scrutiny of all the U frequency spectra shows that the highest probability to observe an inertial domain is found between 1 and 10 Hz. Two examples of typical spectra are shown in Fig. 4. At frequencies higher than 10 Hz, the spectra can be contaminated by noise when turbulence is weak (e.g., right panel of Fig. 4), and by artefacts (multiple peaks) mainly due to motor vibrations of the UAVs, especially during ascents (e.g., left panel of Fig. 4). The characteristics of these contaminations are specific to each UAV and flight, and they can also drift in time due to throttle variations. FLT16-15 was one of the most contaminated among the useful science flights. In practice, for the present purpose, we decided to estimate β from the spectral levels between 1.0 and 7.5 Hz. The spectral slopes between 1.0 and 7.5 Hz were estimated for all the time series of the 39 flights of ShUREX2016 and ShUREX2017. The corresponding histogram is shown in Fig. 5. The mean slope is − 1.64 (i.e., very close to the inertial slope − 5/3). The width of the distribution can be partly due to estimation errors

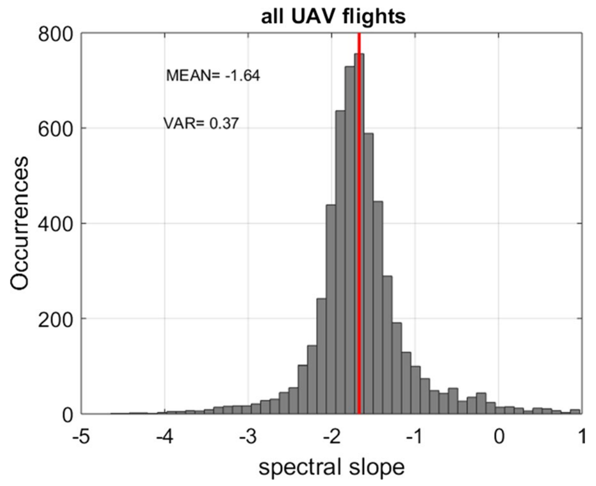

Fig. 5 Histogram of slopes of relative speed spectra calculated in the 1.0–7.5 Hz band for all ShUREX 2016 UAV flights

when estimating slopes on individual spectra. Therefore, from a statistical point of view, the frequency band 1.0–7.5 Hz shows properties consistent with the existence of an inertial subrange.

The second method is based on the selection of spectral bands exhibiting a -5/3 slope in a frequency domain delimited by 0.1 and 40 Hz (arbitrarily) from spectra calculated from time series chunks 50 s in length. The width of the spectral bands is a constant 0.699 decade, e.g., log10(5 Hz)–log10(1 Hz), and 39 overlapping bands are used. For each of these bands, the spectral slope s is estimated from the calculation of the variances in two spectral “sub-bands” of identical relative logarithmic width. An inertial subrange is inferred when $s = -5/3 \pm 0.25$ for at least 3 consecutive spectral bands. The numerical thresholds were chosen in order to fit, as far as possible, the results that would have been obtained from visual inspection of the spectra. In some cases, the criteria may appear too loose or too restrictive, but it appears to be efficient for rejecting most spectral bands affected by instrumental noise and contaminations. A more thorough description of the method and results is in preparation.

The above two methods were applied to ShUREX2016 and ShUREX2017 data and produced the same statistical results.

Figure 6 shows examples of pseudo-vertical ε_U profiles in linear scales during the ascent (A1) and descent (D1) of FLT16-05 and FLT16-08 in altitude ranges covered by MU radar (i.e., above 1.345 km). The profiles are rather distinct during A1 and D1 of FLT16-05, but quite similar during A1 and D1 of FLT16-08. They clearly reveal altitude ranges with multiple peaks of enhanced TKE dissipation rates. These ranges are emphasized by the smoothed profiles shown by the solid and dashed black lines. The former was obtained by using a 30-point rectangular window applied to the time series sampled at 2.5 s (corresponding to 75 s averaging), and the latter by using a Gaussian averaging window. The (non-normalized) Gaussian function was taken as equal to $\exp\left(-z^2/2\alpha^2\right)$, where $\alpha = a/\sqrt{2} = 75/\sqrt{2}\,\mathrm{m}$ in order to fit the characteristics of the expected range weighting function of the MU radar. The two methods provide very similar smoothed profiles. Therefore, the statistics of the comparison results should not depend on the method used for smoothing the ε_U profiles.

Comparisons between ε_U and ε from the radar models

Estimation of L_C

Before comparing ε_U with ε_w and ε_N, estimates of the characteristic scale L_C defined in Eq. (1) can be obtained by replacing ε by ε_U:

$$L_C \approx \left\langle \sigma^2 \right\rangle^{3/2} / \varepsilon_U \tag{8}$$

The left panel of Fig. 7a shows $\left\langle \sigma^2 \right\rangle^{3/2}$ versus ε_U in logarithmic scale for 38 UAV flights (among 39) and all atmospheric conditions. One flight (FLT16-21) was not included due to oversight, and we used it afterwards as a test flight for confirming the statistical results obtained from the 38 flights. The horizontal dashed line in Fig. 7a shows the radar detection threshold (obtained from Fig. 3) and is approximately $\left\langle \sigma^2 \right\rangle^{3/2} = 0.001$. The thick solid line is a straight line of slope 1 and the dashed lines on both sides represent levels 3 times lower or higher. The scatter plot clearly indicates that ε_U appears to be proportional to $\left\langle \sigma^2 \right\rangle^{3/2}$ (especially for the largest values of ε_U), with relatively little scatter along the diagonal. For weak ε_U values ($\varepsilon_U <\sim 10^{-5}\,\mathrm{m}^2\,\mathrm{s}^{-3}$), there is an important bias because the radar estimates are close to the minimum detectable levels and because residual contaminations might be present in the Doppler spectra despite careful data cleaning.

The histogram of $\log_{10}(L_C)$ shown in the right panel of Fig. 7a displays a narrow peak for $\left\langle \sigma^2 \right\rangle^{3/2} > 0.01$ (or for $\varepsilon_U >\sim 10^{-4}\,\mathrm{m}^2\,\mathrm{s}^{-3} = 0.1\,\mathrm{mW\,kg}^{-1}$) with a maximum near ~ 60 m and a mean (median) value of 75 m (61 m). The numerical values depend on the threshold on $\left\langle \sigma^2 \right\rangle^{3/2}$: the mean and median values of L_C increase if the threshold on $\left\langle \sigma^2 \right\rangle^{3/2}$ decreases. However, if the bias observed for $\left\langle \sigma^2 \right\rangle^{3/2} < 0.01$ is only due to instrumental effects, then $L_C \sim 60$–70 m should be representative of all ε_U levels.

From a pragmatic point of view, the analysis shown in Fig. 7a indicates that radar-derived TKE dissipation rates

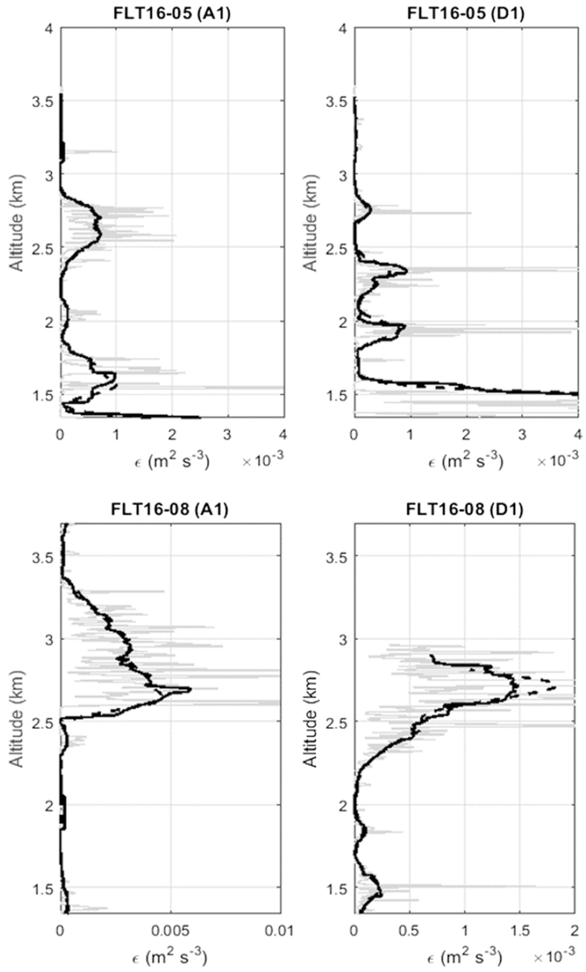

Fig. 6 Examples of the profiles of ε_U for the first 2 ShUREX 2016 science flights (FLT16-05 and FLT16-08) during ascent (A1) and descent (D1). The thick solid and dashed black lines show smoothed profiles with a 30-point running rectangle window and a Gaussian weighting function consistent with the MU radar range weighting function (see text)

(hereafter denoted by ε_R) can be estimated from $\langle\sigma^2\rangle$ using the expression:

$$\varepsilon_R \approx K\left\langle\sigma^2\right\rangle^{3/2} \tag{9}$$

where $K \approx 0.016$ at least for $\langle\sigma^2\rangle^{3/2} > 0.01$ or for $\varepsilon_U >\sim 10^{-4}\,\mathrm{m^2\,s^{-3}}$. From Eq. (9), 50.5% (72.5%, 86.5%) of ε_R estimates do not differ by more than a factor 2 (3, 5) from ε_U estimates. The spectral width is thus the dominant parameter when estimating ε from radar data. We will discuss this result in "Comparisons between ε_U and ε from the radar models" section.

Comparisons between ε_U and ε_R

Figure 8a shows examples of comparison results between ε_U and ε_R profiles for FL16-T05 (A1) and FLT16-08 (A1). The agreements are remarkable. Note that there is about one order of magnitude of difference between the maximum values of TKE dissipation rates observed during FLT16-05 and FL16-T08. Figure 8b shows the result for FLT16-21 (A1). Since this flight was not included in the statistics leading to Eq. (9), these are absolute comparisons and it is the very first attempt at confirmation of Eq. (9). The agreement is again good, both in shape and levels, with a ratio of the two being much less than a factor 2 where ε_U and ε_R are maximum (above 2.5 km). The ε_U profiles fall within the range of variability of ε_R at almost all altitudes.

Figure 9a, b shows the results of comparisons in linear and logarithmic scales for all the 16 ShUREX 2016 and 23 ShUREX 2017 science flights, respectively, concatenated in chronological order. As expected, the largest discrepancies appear in logarithmic scale for small values (due to the minimum detectable value of $\varepsilon_R \sim 0.016 \times 0.001 = 1.6 \times 10^{-5}\,\mathrm{m^2\,s^{-3}}$). Elsewhere, there is almost a one-to-one correspondence between all the peaks. Therefore, both the UAV and the radar detected the same turbulence events with similar ε intensities (assuming the validity of Eq. 9).

The results shown in Figs. 7a, 8 and 9 include all altitudes and all turbulence events, without any distinction between shear-generated and convectively generated turbulence in clear air and cloudy conditions. It is not easy to separate the various turbulence events according to their source or nature, but it is possible to reject the following contributions at altitude ranges from PTU data and radar images:

1. where clouds were observed,
2. associated with cloudy or clear air convective boundary layers (CBL),
3. associated with convective layers underneath clouds [mid-level cloud base turbulence (MCT) layer (e.g., Kudo et al. 2015)].

These events (and clouds) were often associated with the largest values of TKE dissipation rates, but they constituted only 23% of the overall dataset. Thus, the datasets used for the analysis (Fig. 7a) contained mainly turbulence in clear air conditions outside regions potentially affected by cloud dynamics and CBL. Figure 7b shows the results after excluding the convective turbulence events. They do not strongly differ from

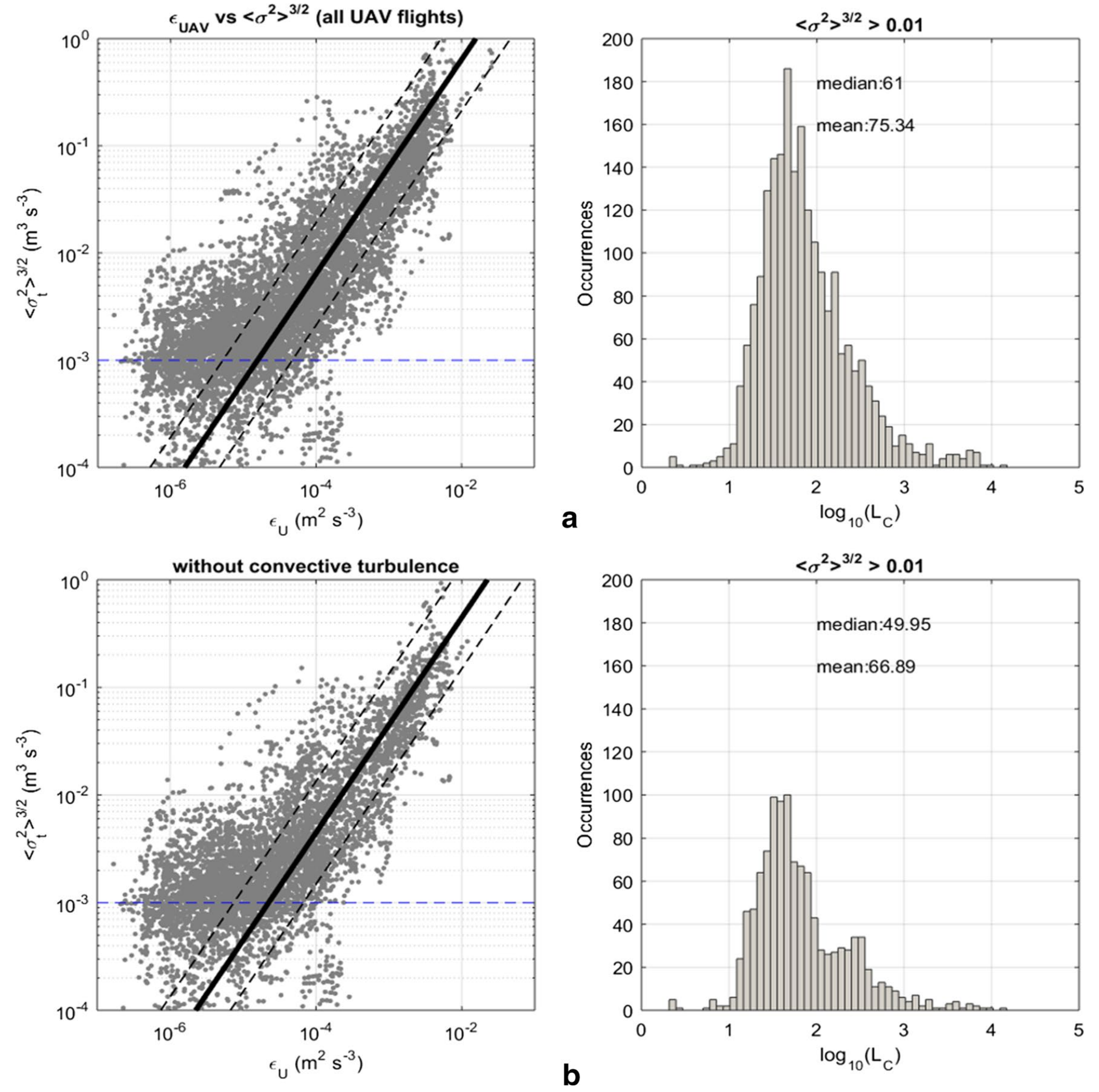

Fig. 7 **a** (Left) Scatter plot of smoothed $\langle\sigma^2\rangle^{3/2}$ versus ε_U for all 2016 and 2017 UAV flights except FLT16-21. σ^2 was calculated as shown in Fig. 2. (Right). The corresponding histogram of the apparent buoyancy scale $\tilde{L}_B$ for $\langle\sigma^2\rangle^{3/2} > 0.01$. **b** Same as **a** after removal of turbulent regions associated with convective boundary layers, clouds and MCT layers

those shown in Fig. 7a, indicating that the observations made from the overall datasets are also representative of the free atmosphere, in the absence of convection. In particular, the σ^3 dependence is still observed, but with slightly smaller values of L_C. The histogram of L_C (right panel of Fig. 7b) seems to have a double-peak distribution. The smaller one may not be representative (because likely due to residual contaminations, see left panel of Fig. 7b). The maximum of the larger distribution is around $L_C \sim 50$ m. Finding a smaller value for stratified conditions only is not surprising since the convective layers are much deeper and should be associated with larger characteristic scales. The difference between the two estimates (60 and 50 m) is not very large, however. We will keep 60 m for the subsequent comparisons.

TKE dissipation rates and isotropy of the radar echoes

Figure 10 shows the scatter plot of ε_R and ε_U versus the radar echo power aspect ratio AR (dB) defined as $\log 10(P_v) - \left(\log 10(P_N) + \log 10(P_E)\right)/2$, where P_v, P_N and P_E are echo power measured in the three radar

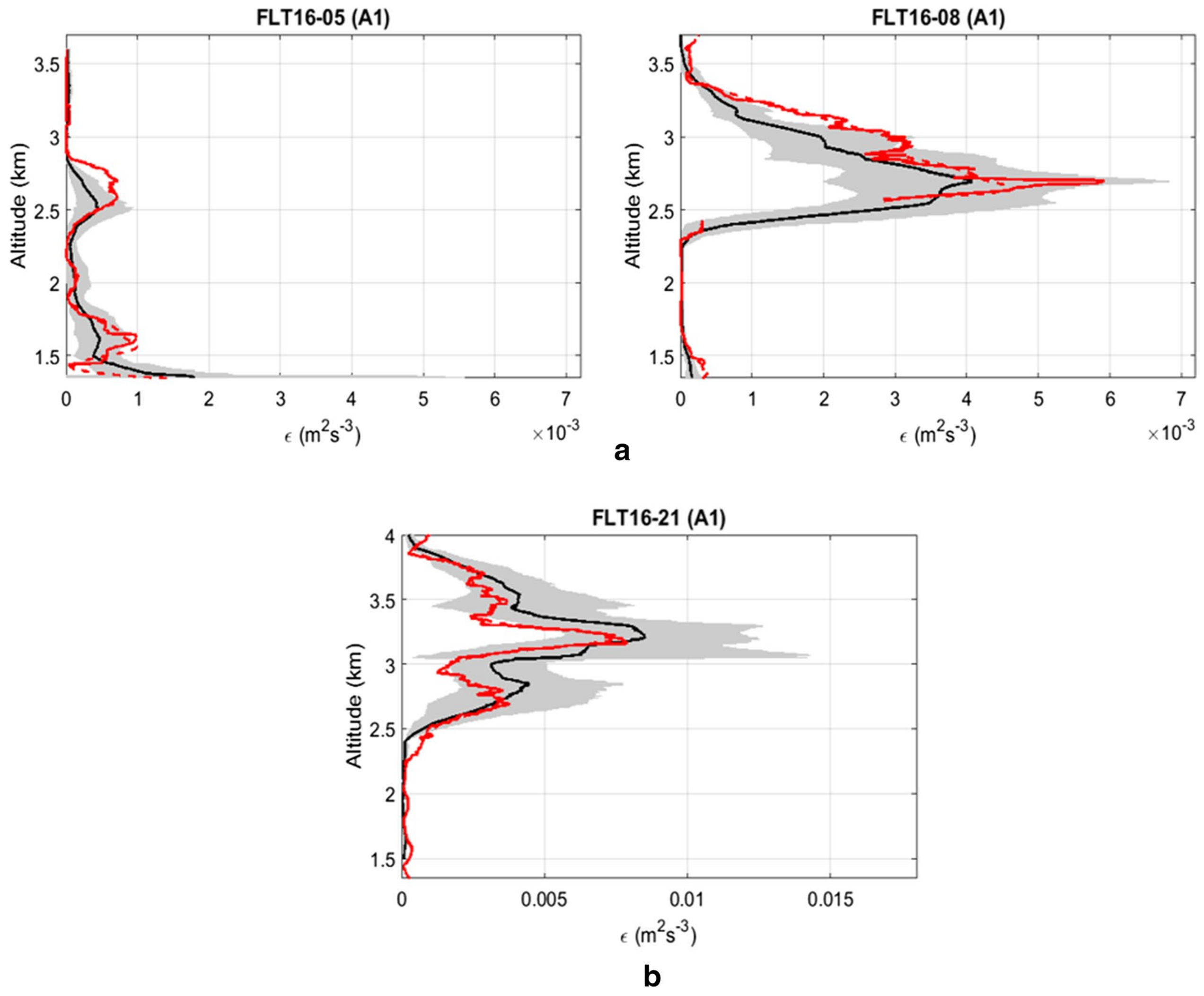

Fig. 8 **a** Comparisons of smoothed profiles of ε_U (red solid and dashed lines) and ε_R (solid line) for FLT16-05 (A1) (left) and FLT16-08 (right). The gray areas show the mean ± rms values of ε_U for the 4 min of time averaging. **b** Same as **a** but or FLT16-21 (A1)

beam directions (vertical, North and East, 10° off zenith). Echo powers were estimated and averaged over 4 min along the UAV flight tracks in the same way as $\langle \sigma^2 \rangle$ (see Fig. 1). A small aspect ratio (say, < 3 dB in absolute value) is generally considered as a signature of scattering from turbulence, which is isotropic or nearly so. This is especially true when the averaging time is short [aspect ratio is a statistical parameter that requires time averaging and horizontal homogeneity hypothesis]. It is striking to note that almost all values of $\varepsilon_U > 1.6 \times 10^{-4}\ \mathrm{m^2\,s^{-3}}$ are associated with $|AR| < 3\,\mathrm{dB}$, i.e., with isotropic echoes. This result is extremely consistent with the fact that the layers of enhanced TKE dissipation rates are associated with relatively deep layers of turbulence, isotropic at the Bragg scale. In such layers, the radar echoes are weakly (or even not) affected by specular reflectors. This result justifies a posteriori the use of data from the vertical beam for estimating $\langle \sigma^2 \rangle$. Incidentally, it is also an additional clue suggesting that the radar and the UAVs indeed detected the same, most prominent, turbulence events. For $\varepsilon_U < 1.6 \times 10^{-4}\ \mathrm{m^2\,s^{-3}}$ (i.e., for the weakest values), AR can be significantly larger than 3 dB. It is difficult to know if this property is due to anisotropic turbulence (consistent with weak turbulence) or due to the coarse resolution of the radar (thin layers of isotropic turbulence surrounded by stable layers within the radar volume).

Comparisons between ε_U and ε_N, ε_W

On the one hand, ε_N was estimated from Eq. (2) by calculating $N^2 = g/T(\mathrm{d}T/\mathrm{d}z + \Gamma_a)$ $(\Gamma_a = 0.001\ \mathrm{K\,m^{-1}})$ from IMET and CWT data at the radar range

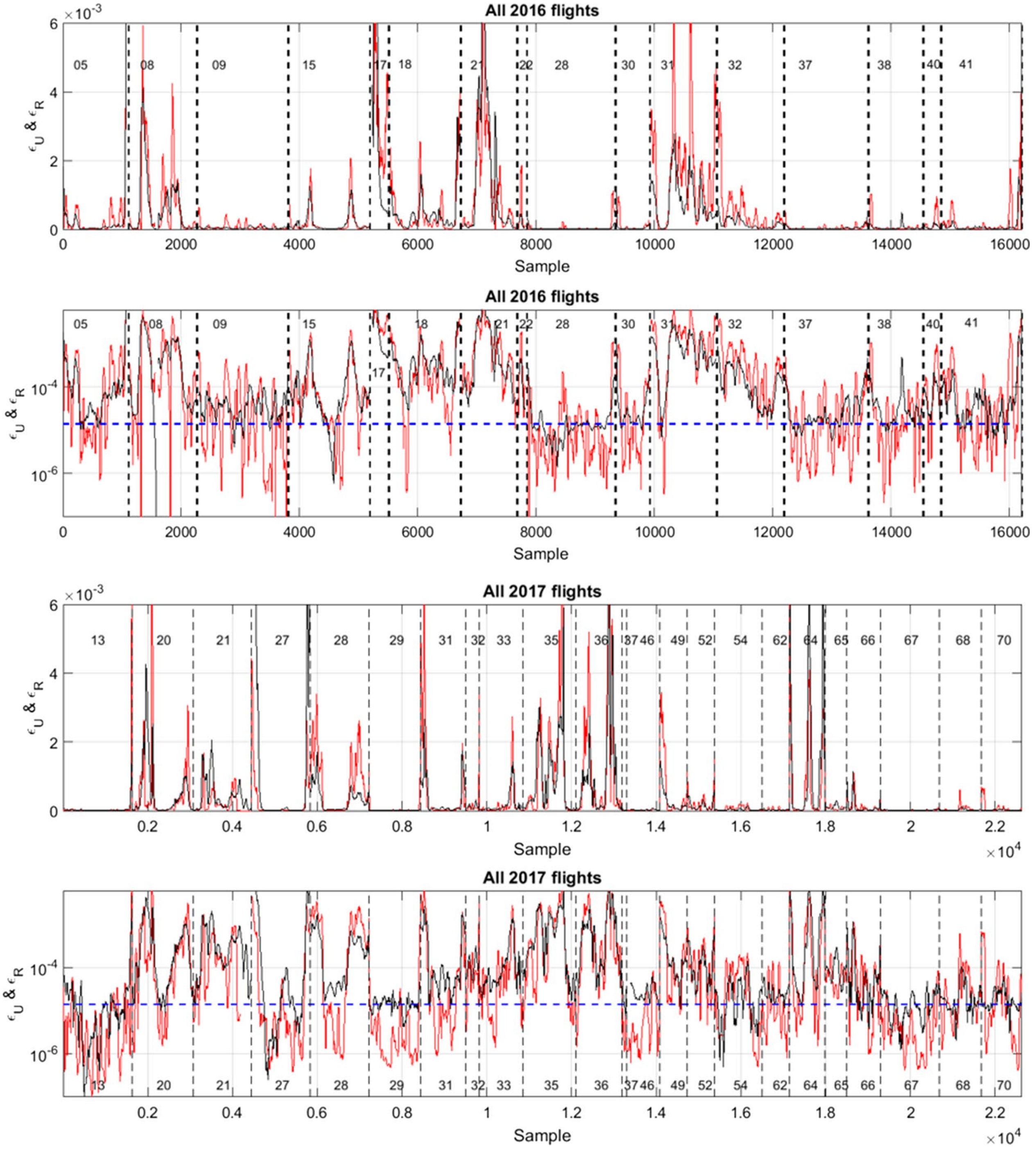

Fig. 9 **a** Concatenation of all ε_U (red) and ε_R(black) profiles from the 2016 UAV flights in chronological order (the vertical dashed lines show the transition between the flights). (Top) linear scale. (Bottom) logarithmic scale. The blue dashed line shows the minimum level (~$1.6\ \times\ 10^{-5}$ m^2 s^{-3}) detectable by the radar according to Fig. 3. **b** Same as **a** for the 2017 flights

resolution (150 m) by applying a low-pass filter with a cutoff of 300 m on the temperature profiles. Examples of N^2 (150 m) profiles estimated from IMET and CWT data for FLT16-05 (A1) and FLT16-08 (A1) are shown in Fig. 11. The *y* reveal that N^2 is positive everywhere during FLT16-05 (A1) and negative in the height range 2.6–3.0 km during FLT16-08 (A1).

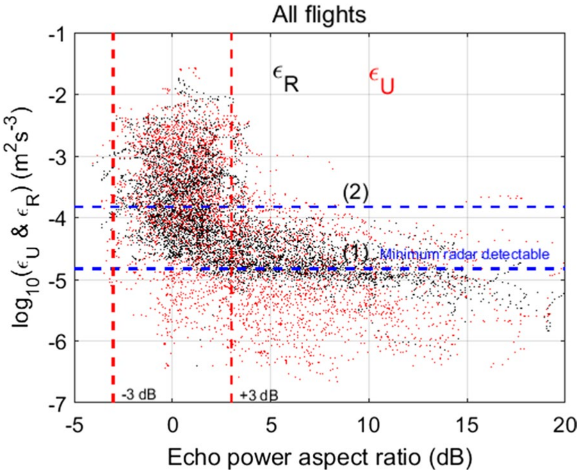

Fig. 10 Radar echo power aspect ratio (dB) defined as $\log 10(P_V) - (\log 10(P_N) + \log 10(P_E))/2$ calculated in the same way as σ^2 ("Theoretical bases and practical methods of ε estimation" section) versus $\log 10(\varepsilon_R)$ (black dots) and $\log 10(\varepsilon_U)$ (red dots). The statistics was made on the ShUREX2016 flights. The blue dashed line (1) shows the minimum ε values detectable by the radar. The blue dotted dashed line shows the level equal to 10 times the minimum threshold

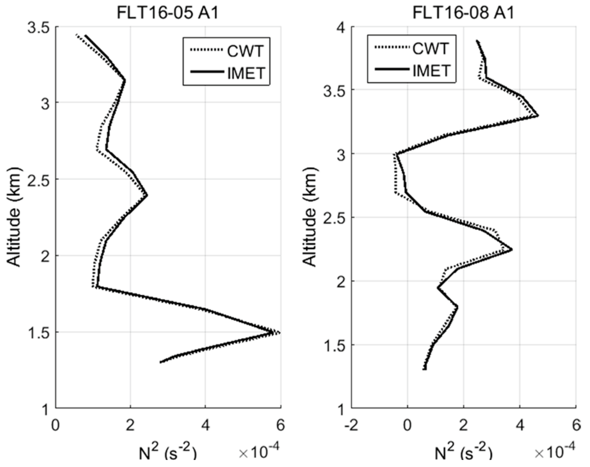

Fig. 11 Vertical profiles of dry N^2 calculated from IMET (solid) and CWT (dotted) sensors at a vertical resolution of 150 m (i.e., the range radar resolution) for FLT16-05 (A1) and FLT16-08 (A1)

On the other hand, ε_W can be estimated from Eq. (3) by performing a numerical integration of I for each altitude z (without L_H).

The top panel of Fig. 12 shows the superposition of ε_U, ε_R, ε_N and ε_W profiles for FLT16-05 (A1) and FLT16-08 (A1). The ε_W profiles appear to be similar to the ε_R profiles but are underestimated, typically by a factor ~ 2 with respect to ε_R (and ε_U) at almost all altitudes and for both cases. The ε_N profiles exhibit more complex features. For FLT16-05 (A1), ε_N shows a good agreement in levels and shape with ε_U. Therefore, from the analysis of a single profile, it can be concluded that ε_N provides reasonable agreement (at least in linear scale). However, for FLT16-08 (A1), ε_N is not defined in the altitude range (2.6-3.0 km) where ε_U, ε_R and ε_W are found to be maximum because N^2 is negative. ε_N is maximum on both sides due to N^2 enhancements at the edges (Fig. 11). Here, ε_N provides radically different information on the turbulent state of the atmosphere between the altitudes of 2.6 km and 3.5 km. The corresponding time-height cross sections of radar echo power at high resolution and at vertical incidence, shown in the bottom panel of Fig. 12, permits us to better understand the differences between FLT16-05 and FLT16-08. During FLT16-05, stratified conditions were clearly observed but were quickly changing between ascent (A1) and descent (D1) (so that ε_U profiles were distinct during A1 and D1, see Fig. 6a). During FLT16-08, the UAV crossed a MCT layer in the altitude range 2.6–3.5 km. MCT layers are basically generated by a convective instability at the cloud base due to evaporative cooling from sublimating precipitation in the sub-cloud layer (e.g., Kudo et al. 2015). For such conditions, $N^2 < 0$ can be observed as is the case here, and N^2 can be enhanced at the edges due to turbulent mixing. Therefore, ε_N fails to reproduce ε_U because it is not defined when $N^2 < 0$ in the core of the layer and because the model is inapplicable to convective turbulence.

Figure 13a, b shows information similar to Fig. 9a, b for all flights and all ascents and descents including ε_N (green line) and ε_W (black line), ε_R and ε_U being shown as red and blue lines, respectively. The figure confirms the tendencies shown in Fig. 12. The series of ε_W values reveals very similar features as the series of ε_R and ε_U with a slight but systematic underestimation. ε_N estimates are apparently consistent with the other estimates but discrepancies, such as those shown in Fig. 12, are difficult to see.

Figure 14 shows the histogram of differences (in logarithmic scales) between ε_R and ε_U (left panel), between ε_W and ε_U (middle panel), and between ε_N and ε_U (right panel), when ε_N is defined (i.e., $N^2 > 0$) for $\varepsilon > 1.6 \times 10^{-5}\,\mathrm{m}^2\,\mathrm{s}^{-3}$. The histogram for $\log_{10}(\varepsilon_R/\varepsilon_U)$ shows a peak close to 0 (by definition). It shows the narrowest peak (minimum standard deviation) among the three estimates. From a statistical point of view, ε_R is thus the best estimate relative to ε_U. The histogram for $\log_{10}(\varepsilon_W/\varepsilon_U)$ shows a slightly wider distribution with a peak around -0.40 indicating an underestimation by a factor ~ 2.5 on average. The histogram for $\log_{10}(\varepsilon_N/\varepsilon_U)$ shows a relatively wide distribution at ~ 0.16 indicating a slight overestimation of 1.44 on average. However, this result, favorable to ε_N, hides an important bias. Figure 15

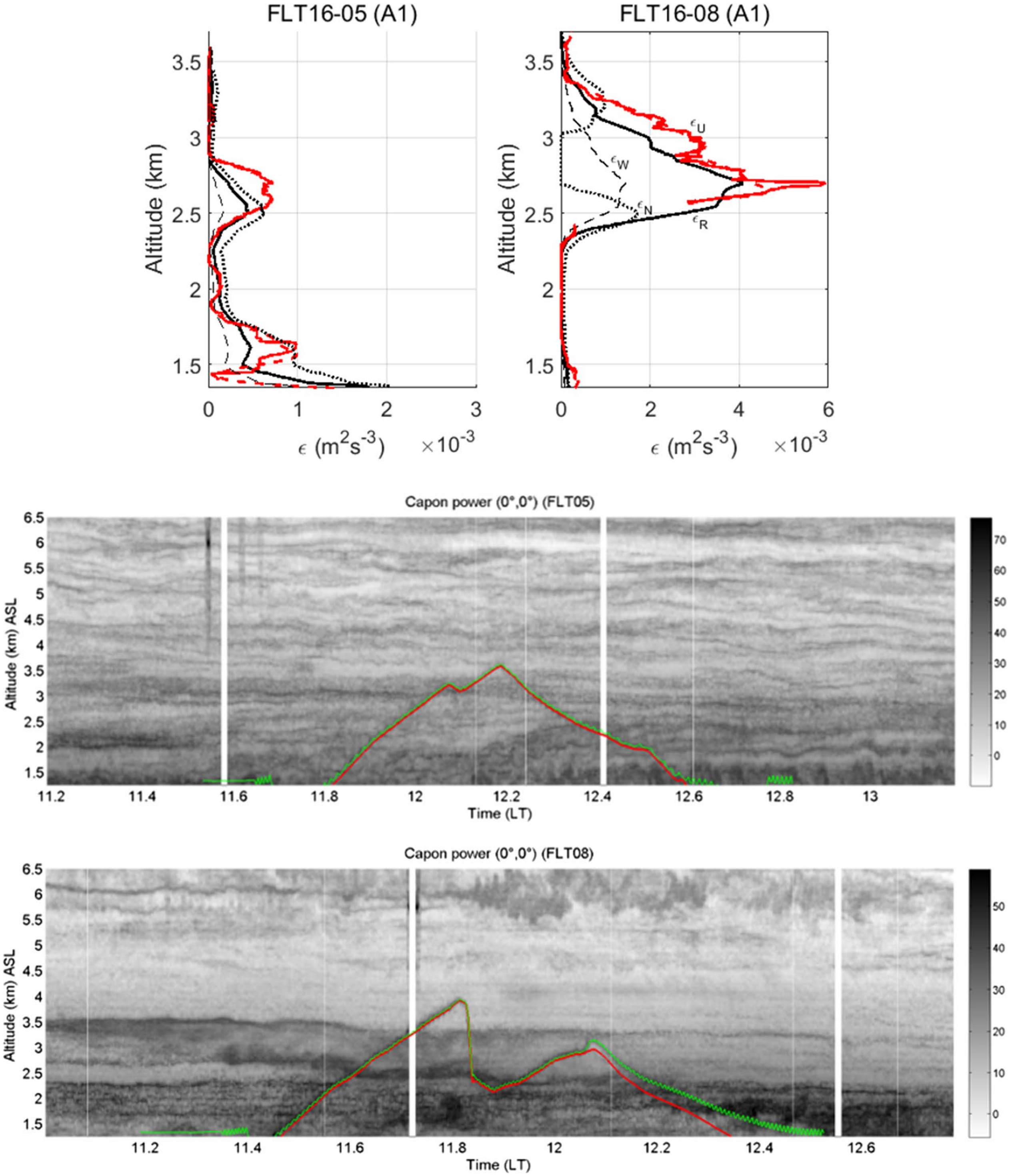

Fig. 12 (Top) Pseudo-vertical profiles of ε_U, ε_R, ε_N and ε_W for FLT16-05 (A1) and FLT16-08 (A1). For legibility, the standard deviation for the radar has been omitted. (Bottom) Time-height cross sections of radar echo power at vertical incidence around the two UAV flights. The green (red) lines show the distance (altitude) of the UAV with respect to the MU radar

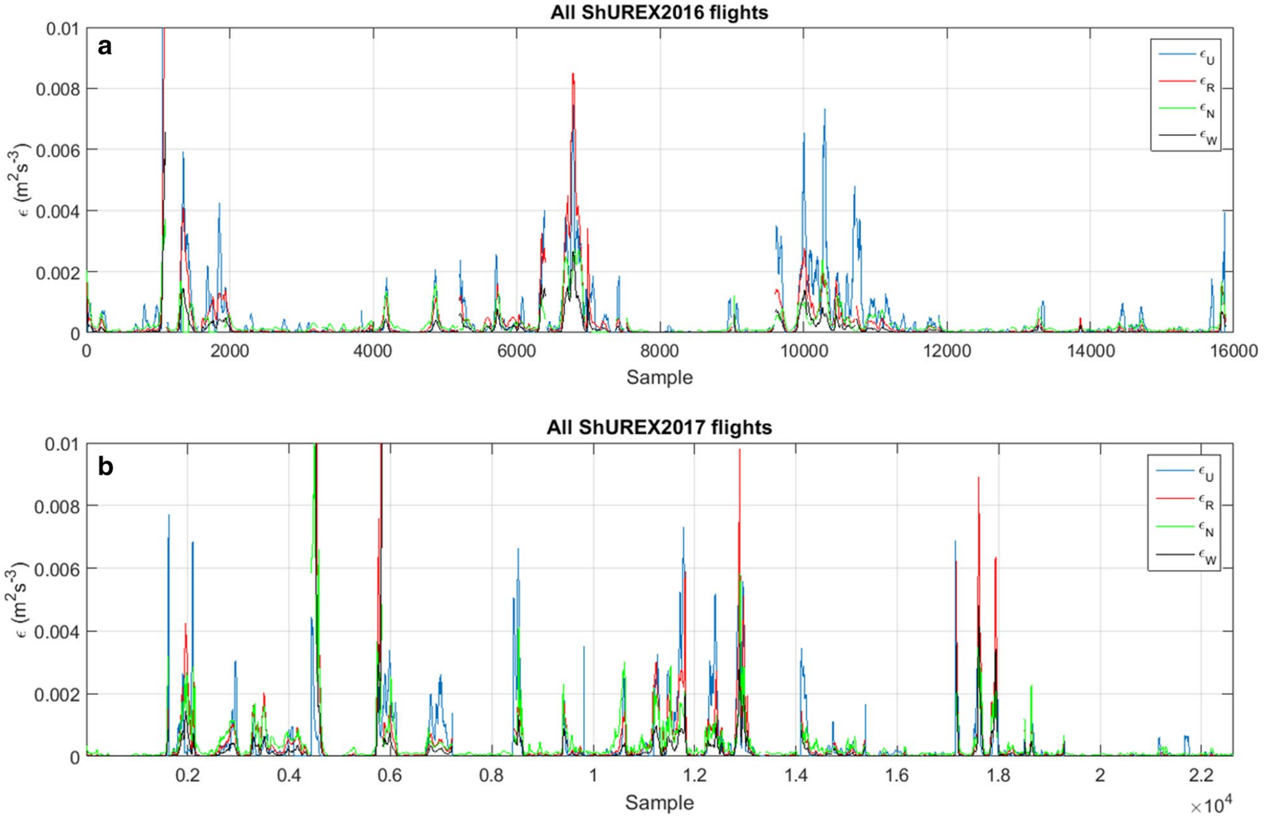

Fig. 13 **a** Concatenation of all ε_U (blue), ε_R (red), ε_W (black) and ε_N (green) profiles from the ShUREX2016 UAV flights in chronological order. **b** Same as **a** for ShUREX2017 UAV flights

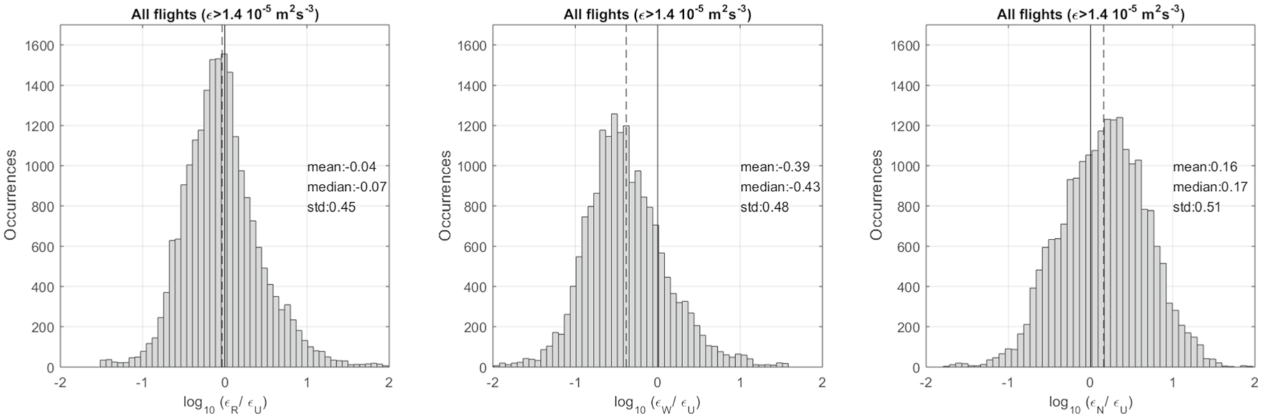

Fig. 14 Histograms of $\log_{10}(\varepsilon_R/\varepsilon_U)$ (left), $\log_{10}(\varepsilon_W/\varepsilon_U)$ (middle), and $\log_{10}(\varepsilon_N/\varepsilon_{UAV})$ (right) corresponding to the values shown in Fig. 13 for all the ShUREX2016 and ShUREX2017 flights

shows the results of regression and correlation analyses between ε_U and the three radar estimates assuming errors on both variables, and after rejecting dissipation rates smaller than $1.6 \times 10^{-5}\,\mathrm{m}^2\,\mathrm{s}^{-3}$ (because of the radar detection threshold and residual contaminations for weak values). The slopes of the regression line are close to 1, 0.91 and 0.92, between $\log_{10}(\varepsilon_U)$ and $\log_{10}(\varepsilon_R)$ and between $\log_{10}(\varepsilon_U)$ and $\log_{10}(\varepsilon_W)$, respectively, confirming reasonably, the σ^3 dependence of TKE dissipation rates. The corresponding correlation

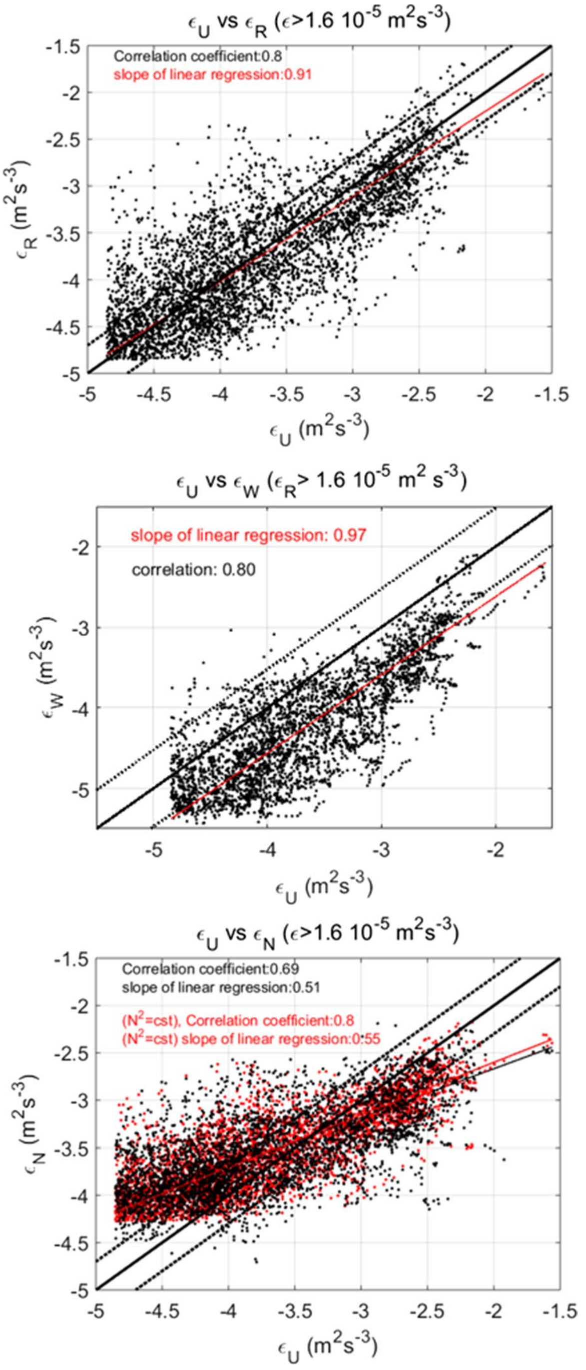

Fig. 15 Scatter plots of ε_U versus ε_R (top), ε_W (middle) and ε_N (bottom) after rejecting values smaller than 1.6×10^{-5} m^2 s^{-3}. The bottom panel shows the results with measured N^2 and with $N^2 = 1.47 \times 10^{-4}$ s^{-2}

coefficients are also nearly identical, at 0.8 and 0.78, respectively. As reported above, the main statistical difference between ε_R and ε_W is the slight bias in levels (factor ~ 2.5 with ε_U). In contrast, the regression analysis between $\log_{10}(\varepsilon_U)$ and $\log_{10}(\varepsilon_N)$ leads to a slope of 0.51 and the correlation coefficient is significantly smaller (0.69). Therefore, as expected, the model producing ε_N is not suitable, because it predicts a σ^2 dependence of ε. Although correct in average, the model tends to overestimate ε for $\varepsilon_U <\sim 4 \times 10^{-4}$ m^2 s^{-3} and to underestimate ε for $\varepsilon_U >\sim 4 \times 10^{-4}$ m^2 s^{-3}. Note that detection threshold effects cannot explain the largest biases for small values, since the associated values were rejected by the regression analysis (but not in Fig. 13). The scatter plot obtained with a constant value of N^2 equal to the mean value for the stratified regions sampled by the UAVs ($= 1.47 \times 10^{-4}$ s^{-2}), is superimposed to the bottom panel of Fig. 15 (red dots). The regression slope is very similar but the correlation coefficient is improved (0.8). Therefore, the tendency shown by the model producing ε_N does not depend on an accurate estimate of N^2.

Discussions

Our statistical results suggest that the TKE dissipation rates estimated from the MU radar operated at a range resolution of 150 m and a beam aperture of 1.32° are proportional to σ^3, for all atmospheric conditions in the lower atmosphere (up to ~ 4.0 km). The σ^3 dependence is consistent with the results reported by Chen (1974) who showed from data collected by airplanes that TKE dissipation rates are proportional to $\left\langle w'^2 \right\rangle^{3/2}$ at stratospheric heights. To some extent, it is also consistent with results reported by Bertin et al. (1997), who performed similar studies for stratospheric heights with the UHF Proust radar and high-resolution balloon data. However, partly due to the small amount of data, they suggest both σ^2 and σ^3 dependences for the same dataset (their Figs. 7b, 8). Jacoby-Koaly et al. (2002) compared TKE dissipation rates estimated from UHF (1238 MHz) radar and airplane data in CBL at a vertical resolution of 150 m by using the White et al. formulation. They found good statistical agreements (at least when using data from oblique beams, because data collected from the vertical beam were contaminated by ground clutter). McCaffrey et al. (2017) also compared dissipation rates estimated in the planetary boundary layer from two UHF (449 MHz and 915 MHz) radars using the White et al. (1999) model with values estimated from sonic anemometers mounted on a 300 m tower. Their results also tend to confirm a σ^3 dependence for turbulence in the CBL.

In the present work, the ε_N model was found to be inadequate, although it has also been widely used with VHF radar observations (e.g., Hocking 1983, 1985, 1986, 1999, Fukao et al. 1994; Delage et al. 1997; Nastrom and Eaton 1997; Fukao et al. 2011, among many others). However, *on average*, and for stratified conditions, the model producing ε_N provides reasonable agreements with ε_U, but it tends to overestimate (underestimate) TKE dissipation rates when turbulence is weak (large). Li et al. (2016) compared ε_N values obtained with the 53.5 MHz MAARSY radar at tropo-stratospheric heights with indirect estimates of dissipation rates from balloon data using a Thorpe analysis. Considering all the possible sources of discrepancies, the agreement was satisfying but the approach was likely not adapted for validating ε_N since the estimates from balloon data were themselves based on a model. Deghan et al. (2014) made studies similar to those presented here with a 40.68 MHz VHF radar and airplane observations mainly in the boundary layer. They also found reasonable agreements between ε_N and dissipation rates estimated from aircraft measurements (their Figs. 8, 12), sometimes with some noticeable difference in levels (a factor 5 in Fig. 12) and at coarser range resolution (500 m). In addition, they used standard values of N^2 for some comparisons. This dataset may not have been sufficiently large for highlighting the biases produced by the model producing ε_N so that our respective results are not necessarily incompatible.

Conclusions

TKE dissipation rates ε were estimated from measurements made by high-frequency response Pitot sensors onboard UAVs and from MU radar Doppler spectra in the lower troposphere (up to ~ 4.0 km). The comparisons showed that:

(a) Maxima of ε ($\sim 10^{-5} - 10^{-2}\,\mathrm{m}^2\,\mathrm{s}^{-3}$ typically, or $\sim 0.01 - 10\,\mathrm{mW\,kg}^{-1}$) were observed at the same altitudes and times by the UAV and the radar indicating that the same turbulence events were generally sampled by both instruments at a horizontal distance of 1.0 km or less. Conditions were thus favorable to test the standard models used for estimating ε from radar data.

(b) ε_U was found to be proportional to σ^3, not σ^2 as expected for stably stratified turbulence. The best agreement in turbulence levels was found by assuming that $\varepsilon_U = K\sigma^3$ with $K \sim 0.016$. This surprisingly elementary model is equivalent to assuming a characteristic scale L_C of the order of 50–70 m. This scale is not necessarily related to an effective outer scale of turbulence because it seems to be appropriate for all cases, convectively or shear-generated turbulence, in deep convective layers or in stratified conditions. Therefore, it is likely not relevant to compare this scale (defined from dimensional analysis) with the dimensions $2a$, $2b$ of the radar sampling volume ($2b$ = 150 m, $2a$ = [53 m–156 m] in the height range 1.3–4.0 km) for selecting the right model. More refined analyses are necessary in order to know if there are really consistency problems or not. From a pragmatic point of view, this simple model can be used for estimating ε solely from measurements of VHF radar Doppler spectral width. It is likely accurate enough for climatological studies without the need for additional measurements of N^2, at least for low tropospheric altitudes. All ε_U values larger than $\sim 1.6 \times 10^{-4}\,\mathrm{m}^2\,\mathrm{s}^{-3}$ ($\sim 0.16\,\mathrm{mW\,kg}^{-1}$) were found to be associated with weak radar aspect ratios ($|AR| < 3\,\mathrm{dB}$), which can reasonably be interpreted as backscatter from isotropic turbulence. It is thus consistent and justifies the use of Doppler spectra from the vertical beam when not altered by ground clutter. It means that data from oblique beams do not need to be used for estimating ε from radar data, even as weak as those reported in the present study and even at a vertical resolution of 150 m. The use of Doppler spectra measured from oblique directions requires many more corrections and accurate knowledge of horizontal wind shear, which can be the cause of additional uncertainties when estimating the Doppler variance produced by turbulence.

(c) The key finding described in (b) does not mean that the Weinstock (1981) model adapted by Hocking (1983) is always irrelevant for stratified conditions. But it is likely not suitable for lower troposphere observations at a range resolution of 150 m with the MU radar and for the observed range of ε values.

(d) ε_W, based on the formulation proposed by Frisch and Clifford (1974) and subsequent authors, is also suitable since it predicts a σ^3 dependence. However, it is a slight underestimate with respect to ε_U ($\varepsilon_U \sim 2.2\varepsilon_W$ in average) but is not biased.

(e) Finally, ε_R and ε_W were found consistent with ε_U in convective regions (such as MCT and CBL) while ε_N failed to reproduce the correct levels in the core and at the edges of the convectively generated turbulent layers. This is an additional argument for avoiding a systematic use of ε_N in the free atmosphere. Nevertheless, if used, climatological values of N^2 seem to be preferable to measured values.

Abbreviations

AR: aspect ratio; ASL: above sea level; CBL: convective boundary layer; CU: Colorado University; CWT: cold wire temperature; IMET: international met (systems); KOC: Kolmogorov–Obukhov–Corrsin; MCT: mid-level cloud base turbulence; ST: stratosphere troposphere; MU: middle and upper atmosphere; PTU: pressure temperature humidity; ShUREX: Shigaraki UAV radar experiment; SNR: signal-to-noise ratio; TKE: turbulence kinetic energy; UHF: ultra-high frequency; VHF: very high frequency; UAV: unmanned aerial vehicle.

Authors' contributions

HL performed all the radar and UAV data processing with assistance from HH and DL. LK led the ShUREX campaign and participated in the analysis and synthesis of the study results. DL was responsible for collection of the UAV data and AD provided the useable UAV data of ShUREX2017. All authors read and approved the final manuscript.

Author details

[1] Mediterranean Institute of Oceanography (MIO), UM 110, UMR 7294, Université de Toulon, La Garde, France. [2] Department of Aerospace Engineering Sciences, University of Colorado, Boulder, CO, USA. [3] Research Institute for Sustainable Humanosphere, Kyoto University, Kyoto, Japan.

Acknowledgements

This study was supported by JSPS KAKENHI Grant No. JP15K13568 and the research Grant for Mission Research on Sustainable Humanosphere from Research Institute for Sustainable Humanosphere (RISH), Kyoto University. The MU radar belongs to and is operated by RISH, Kyoto University. The authors thank T. Mixa, M. Yabuki, R. Wilson and T. Tsuda for their cooperation during the campaigns and thank N. Nishi (Fukuoka University) for his kind assistance during the revision of the manuscript and his supply of meteorological data used for reviewers' reply.

Competing interests

The authors declare that they have no competing interests.

Funding

This study was supported by JSPS KAKENHI Grant No. JP15K13568 and the research Grant for Mission Research on Sustainable Humanosphere from Research Institute for Sustainable Humanosphere (RISH), Kyoto University. It was also partly supported by the US National Science Foundation (Grant No. AGS 1632829). The MU radar belongs to and is operated by RISH, Kyoto University.

Appendix: Practical estimation of Eq. (6)

In this appendix, the detailed procedure used for obtaining Eq. (6) is given.

The Doppler spectra are first calculated for each of the 128 radar gates from complex time series of 128 points weighted by a Hanning window. The noise level for each radar gate is then estimated from Hildebrandt and Sekhon's method. The noise profile of 128 points is sorted and the average of the 3 smallest values are used a proxy of the noise level for all the radar gates. The moment method is then used to estimate the primary parameters (power, Doppler shift and spectral width). Because the Doppler spectra can be contaminated by any kind of outliers and in particular, UAV echoes (see Luce et al. 2017), all the Doppler spectra have been edited and manually corrected in order to reject, as far as possible, these contaminations. Most of time, the Doppler shift of UAV echoes did not coincide with the Doppler shift of atmospheric echoes, so that it was possible to reject these echoes by Doppler sorting. The rejection consisted in replacing the Doppler ranges on both sides of clear air atmospheric peak by the average noise power density defined above. The moment method was finally applied again, in order to get the definitive estimates of the primary parameters.

The turbulent component of the Doppler variance was then calculated as follows. The measured spectral half width (i.e., σ_m) is first converted to half power:

$$\sigma_{1/2} = \sqrt{2\ln 2} \times \sigma_m \tag{10}$$

After beam-broadening correction ($\sigma_b^2 = \left(\bar{U}\theta_0\right)^2$), we obtain:

$$\sigma_{BB}^2 = \sigma_{1/2}^2 - \left(\bar{U}\theta_0\right)^2 \tag{11}$$

where $\theta_0 = 1.32°$ for the MU radar (e.g., Fukao et al. 1994) and $\bar{U}$ is the mean wind speed estimated from the MU radar by using the 3 radial components. The time averaging was applied over Ta ~ 100 s (in practice, the results did not strongly depend on the choice of Ta). Finally, the Doppler variance due to turbulence is:

$$\sigma^2 = \sigma_{BB}^2/(2\ln 2) \tag{12}$$

Received: 28 June 2018 Accepted: 15 December 2018

References

Bertin F, Barat J, Wilson R (1997) Energy dissipation rates, eddy diffusivity, and the Prandtl number: an in situ experimental approach and its consequences on radar estimate of turbulent parameters. Radio Sci 32:791–804

Chapman D, Browning KA (2001) Measurements of dissipation rate in frontal zones. Q J R Meteorol Soc 127:1939–1959

Chen WY (1974) Energy dissipation rates of free atmospheric turbulence. J Atmos Sci 31:2222–2225

Cohn SA (1995) Radar measurements of turbulent eddy dissipation rate in the troposphere: a comparison of techniques. J Atmos Ocean Technol 12:85–95

Dehghan A, Hocking WK (2011) Instrumental errors in spectral-width turbulence measurements by radars. J Atmos Sol Terr Phys 73:1052–1068

Dehghan A, Hocking WK, Srinivasan R (2014) Comparisons between multiple in situ aircraft turbulence measurements and radar in the troposphere. J Atmos Sol Terr Phys 118:64–77

Delage D, Roca R, Bertin F, Delcourt J, Crémieu A, Masseboeuf M, Ney R (1997) A consistency check of three radar methods for monitoring eddy diffusion and energy dissipation rates through the tropopause. Radio Sci 32:757–767

Doviak RJ, Zrnic' DS (1993) Doppler radar and weather observations. Academic, San Diego, CA, p 562

Frehlich R, Meillier Y, Jensen MA, Balsley BB (2003) Turbulence measurements with the CIRES tethered lifting system during CASES-99: calibration and spectral analysis of temperature and velocity. J Atmos Sci 60:2487–2495

Frisch AS, Clifford SF (1974) A study of convection capped by a stable layer using Doppler radar and acoustic echo sounders. J Atmos Sci 31:1622–1628

Fukao S, Sato T, Tsuda T, Yamamoto M, Yamanaka MD (1990) MU radar—new capabilities and system calibrations. Radio Sci 25:477–485

Fukao S, Yamanaka MD, Ao N, Hocking WK, Sato T, Yamamoto M, Nakamura T, Tsuda T, Kato S (1994) Seasonal variability of vertical eddy diffusivity in the middle atmosphere. 1. Three-year observations by the middle and upper atmosphere radar. J Geophys Res Atmos 99:18973–18987

Fukao S, Luce H, Mega T, Yamamoto MK (2011) Extensive studies of large-amplitude Kelvin–Helmholtz billows in the lower atmosphere with the VHF middle and upper atmosphere radar (MUR). Q J R Meteorol Soc 137:1019–1041

Gage KS, Balsley BB (1978) Doppler radar probing of the clear atmosphere. Bull Am Meteorol Soc 59:1074–1093

Gossard EE, Chadwick RB, Neff WD, Moran KP (1982) The use of ground-based Doppler radars to measure gradients, fluxes and structure parameters in elevated layers. J Appl Meteorol 21:211–226

Hocking WK (1983) On the extraction of atmospheric turbulence parameters from radar backscatter Doppler spectra. I. Theory. J Atmos Terr Phys 45:89–102

Hocking WK (1985) Measurement of turbulent energy dissipation rates in the middle atmosphere by radar techniques: a review. Radio Sci 20:1403–1422

Hocking WK (1986) Observations and measurements of turbulence in the middle atmosphere with a VHF radar. J Atmos Terr Phys 48:655–670

Hocking WK (1999) The dynamical parameters of turbulence theory as they apply to middle atmosphere studies. Earth Planets Space 51:525–541. https://doi.org/10.1186/BF03353213

Hocking WK, Röttger J, Palmer RD, Sato T, Chilson PB (2016) Atmospheric radar. Cambridge University Press, Cambridge

Hocking WK, Hamza AM (1997) A quantitative measure of the degree of anisotropy of turbulence in terms of atmospheric parameters, with particular relevance to radar studies. J Atmos Sol Terr Phys 59:1011–1020

Hocking WK, Mu PKL (1997) Upper and middle tropospheric kinetic energy dissipation rates from measurements of C_n^2—review of theories, in situ investigations, and experimental studies using the Buckland Park atmospheric radar in Australia. J Atmos Sol Terr Phys 59:1779–1803

Jacoby-Koaly S, Campistron B, Bernard S, Bénech B, Ardhuin-Girard F, Dessens J, Dupont E, Carissimo B (2002) Turbulent dissipation rate in the boundary layer via UHF wind profiler Doppler spectral width measurements. Bound Layer Meterol 103:3061–3389

Kantha L, Lawrence D, Luce H, Hashiguchi H, Tsuda T, Wilson R, Mixa T, Yabuki M (2017) Shigaraki UAV-Radar Experiment (ShUREX 2015): an overview of the campaign with some preliminary results. Prog Earth Planet Sci 4:19. https://doi.org/10.1186/s40645-017-0133-x

Kantha L, Luce H, Hashiguchi H (2018) A note on an improved model for extracting TKE dissipation rate from VHF radar spectral width. Earth Planets Space **(in press)**

Kudo A, Luce H, Hashiguchi H, Wilson R (2015) Convective instability underneath midlevel clouds: comparisons between numerical simulations and VHF radar observations. J Appl Meteorol Clim 54:2217–2227

Kurosaki S, Yamanaka MD, Hashiguchi H, Sato T, Fukao S (1996) Vertical eddy diffusivity in the lower and middle atmosphere: a climatology based on the MU radar observations during 1986–1992. J Atmos Sol Terr Phys 58:727–734

Labitt M (1979) Some basic relations concerning the radar measurements of air turbulence. MIT Lincoln Laboratory, ATC working paper no. 46WP-5001

Lawrence DA, Balsley BB (2013) High-resolution atmospheric sensing of multiple atmospheric variables using the DataHawk small airborne measurement system. J Atmos Ocean Technol 30:2352–2366

Li Q, Rapp M, Schrön A, Scneider A, Stober G (2016) Derivation of turbulent energy dissipation rate with the middle atmosphere alomar radar system (MAARSY) and radiosondes at Andoya, Norway. Ann Geophys 34:1029–1229

Luce H, Hassenpflug G, Yamamoto M, Fukao S (2006) High-resolution vertical imaging of the troposphere and lower stratosphere using the new MU radar system. Ann Geophys 24:791–805

Luce H, Kantha L, Hashiguchi H, Lawrence D, Yabuki M, Tsuda T, Mixa T (2017) Comparisons between high-resolution profiles of squared refractive index gradient M^2 measured by the MU radar and UAVs during the ShUREX 2015 campaign. Ann Geophys 35:423–441

Luce H, Kantha L, Hashiguchi H, Lawrence D, Mixa T, Yabuki M, Tsuda T (2018) Vertical structure of the lower troposphere derived from MU radar, unmanned aerial vehicle, and balloon measurements during ShUREX 2015. Prog Earth Plan Sci 5:29. https://doi.org/10.1186/s40645-018-0187-4

McCaffrey K, Bianco L, Wilczak J (2017) Improved observations of turbulence dissipation rates from wind profiling radars. Atmos Meas Technol 10:2595–2611

Naström GD (1997) Dopplser radar spectral width broadening due to beamwidth and wind shear. Ann Geophys 15:786–796

Nastrom GD, Eaton FD (1997) Turbulence eddy dissipation rates from radar observations at 5–20 km at White Sands Missile Range, New Mexico. J Geophys Res Atmos 102:19495–19505

Sato T, Woodman RF (1982) Fine altitude resolution observations of stratospheric turbulent layers by the Arecibo 430 MHz radar. J Atmos Sci 39:2546–2552

Scipión DE, Lawrence DA, Milla MA, Woodman RF, Lume DA, Balsley BB (2016) Simultaneous observations of structure function parameter of refractive index using a high-resolution radar and the DataHawk small airborne measurement system. Ann Geophys 34:767–780. https://doi.org/10.5194/angeo-34-767-2016

Siebert H, Lehmann K, Wendisch M (2006) Observations of small-scale turbulence and energy dissipation rates in the cloudy boundary layer. J Atmos Sci 63:1451–1466

Tatarski I (1961) Wave propagation in a turbulent medium. Translated by R. A. Silvermann. Graw-Hill, New York

Tsuda T, May PT, Sato T, Kato S, Fukao S (1988) Simultaneous observations of reflection echoes and refractive index gradient in the troposphere and lower stratosphere. Radio Sci 23:655–665

Weinstock J (1978a) On the theory of turbulence in the buoyancy subrange of stably stratified flows. J Atmos Sci 35:634–649

Weinstock J (1978b) Vertical turbulence diffusion in a stably stratified fluid. J Atmos Sci 35:1022–1027

Weinstock J (1981) Energy dissipation rates of turbulence in the stable free atmosphere. J Atmos Sci 38:880–883

White AB, Lataitis RJ, Lawrence RS (1999) Space and time filtering of remotely sensed velocity turbulence. J Atmos Sci 16:1967–1972

Wilson R, Dalaudier F, Bertin F (2005) Estimation of the turbulent fraction in the free atmosphere from MST radar measurements. J Atmos Ocean Technol 22:1326–1339

Yamamoto M, Sato T, May PT, Tsuda T, Fukao S, Kato S (1988) Estimation error of spectral parameters of mesosphere–stratosphere–troposphere radars obtained by least squares fitting method and its lower bound. Radio Sci 23:1013–1021